

UCLA

UCLA Previously Published Works

Title

Quantitative In Vivo Imaging of the Androgen Receptor Axis Reveals Degree of Prostate Cancer Radiotherapy Response.

Permalink

<https://escholarship.org/uc/item/2d7518gk>

Journal

Cell growth & differentiation : the molecular biology journal of the American Association for Cancer Research, 21(4)

Authors

Storey, Claire

Altai, Mohamed

Bicak, Mesude

et al.

Publication Date

2023-04-01

DOI

10.1158/1541-7786.MCR-22-0736

Peer reviewed



Published in final edited form as:

Mol Cancer Res. 2023 April 01; 21(4): 307–315. doi:10.1158/1541-7786.MCR-22-0736.

Quantitative In Vivo Imaging of the Androgen Receptor Axis Reveals Degree of Prostate Cancer Radiotherapy Response

Claire M Storey¹, Mohamed Altai², Mesude Bicak³, Darren R Veach⁴, Katharina Lückerath⁵, Gabriel Adrian², Michael R McDevitt⁴, Teja Kalidindi⁴, Julie E Park¹, Ken Herrmann⁵, Diane Abou^{6,7}, Wahed Zedan², Norbert Peekhaus², Robert J Klein⁸, Robert Damoiseaux^{1,9}, Steven M Larson^{4,10}, Hans Lilja^{11,12,13,14}, Daniel Thorek^{6,7,15}, David Ulmert^{1,2,9,16,17,18}

¹Department of Molecular & Medical Pharmacology, University of California Los Angeles (UCLA), Los Angeles, USA

²Division of Oncology and Pathology, Department of Clinical Sciences, Lund University, Lund, Sweden

³Hasso Plattner Institute for Digital Health, Department of Genetics and Genomic Sciences, Icahn School of Medicine at Mount Sinai, New York, USA

⁴Department of Radiology, Memorial Sloan Kettering Cancer Center (MSKCC), New York, USA

⁵Department of Nuclear Medicine, University Hospital Essen, University of Duisburg-Essen, DKTK, Essen, Germany

⁶Department of Radiology, Washington University School of Medicine, St. Louis, USA

⁷Siteman Cancer Center, Washington University School of Medicine, St. Louis, USA

⁸Icahn Institute for Genomics and Multiscale Biology, Department of Genetics and Genomic Sciences, Icahn School of Medicine at Mount Sinai, New York, USA

⁹California NanoSystems Institute, UCLA, Los Angeles, USA

¹⁰Department of Radiology, Weill Cornell Medical College, New York, USA

¹¹Genitourinary Oncology Service, Department of Medicine, MSKCC, New York, USA

¹²Urology Service, Department of Surgery, MSKCC, New York, USA

¹³Department of Laboratory Medicine, MSKCC, New York, USA

¹⁴Department of Translational Medicine, Lund University, Malmö, Sweden

¹⁵Department of Biomedical Engineering, Washington University School of Medicine, St. Louis, USA

¹⁶Department of Urology, Institute of Urologic Oncology, UCLA, Los Angeles, USA

Corresponding author: David Ulmert, 650 Charles E Young Drive S, Los Angeles, CA 90095, USA, Telephone: +1-310-825-9974, hulmert@mednet.ucla.edu.

Conflict of interest disclosure:

The other authors declare no potential conflicts of interest.

¹⁷Jonsson Comprehensive Cancer Center, David Geffen School of Medicine, UCLA, Los Angeles, USA

¹⁸Eli and Edythe Broad Center of Regenerative Medicine and Stem Cell Research, UCLA, Los Angeles, USA

Abstract

Non-invasive biomarkers for androgen receptor (AR) pathway activation are urgently needed to better monitor patient response to prostate cancer (PCa) therapies. AR is a critical driver and mediator of resistance of PCa but currently available non-invasive PCa biomarkers to monitor AR activity are discordant with downstream AR pathway activity. External beam radiotherapy (EBRT) remains a common treatment for all stages of PCa, and DNA damage induced by EBRT upregulates AR pathway activity to promote therapeutic resistance. [⁸⁹Zr]11B6-PET is a novel modality targeting prostate-specific protein human kallikrein 2 (hK2), which is a surrogate biomarker for AR activity. Here, we studied if [⁸⁹Zr]11B6-PET can accurately assess EBRT-induced AR activity.

Genetic and human PCa mouse models received EBRT (2–50 Gy) and treatment response was monitored by [⁸⁹Zr]11B6-PET/CT. Radiotracer uptake and expression of AR and AR target genes was quantified in resected tissue.

EBRT increased AR pathway activity and [⁸⁹Zr]11B6 uptake in LNCaP-AR and 22RV1 tumors. EBRT increased prostate-specific [⁸⁹Zr]11B6 uptake in PCa-bearing mice (Hi-*Myc* x Pb-*KLK2*) with no significant changes in uptake in healthy (Pb-*KLK2*) mice, and this correlated with hK2 protein levels.

Keywords

hK2; 11B6; prostate cancer; androgen receptor; EBRT; response monitoring

Introduction

External beam radiotherapy (EBRT), a mainstay in PCa therapy, activates AR; this increases the expression of DNA repair genes, which may promote radio-resistance^{1–4} and explain the synergy between ionizing radiation and AR signaling inhibitors (ARSI)^{5,6}. Non-invasive biomarkers for monitoring DNA damage-induced AR activity may allow monitoring response to EBRT and early detection of treatment resistance, and thus, providing PCa patients with individualized treatment options. In the clinical setting, AR activity is currently monitored through the assessment of serum prostate specific antigen (PSA, *KLK3*) levels over time⁷. However, measurements of serum kallikreins provide limited information as they reflect a global average of multiple heterogenic lesions in the metastatic setting with limited correlation to protein production⁸. The development of imaging-based response criteria (RECIST, PERCIST) reflects this challenge; the increasing application of RECIST/PERCIST for assessing response (to radionuclide therapies) - for example in the VISION trial, in which blood PSA levels were a secondary endpoint only – supports the relevance of

these criteria. The capacity to decipher which lesions at which anatomical sites respond and which do not respond would significantly augment future patient management.

Similar to PSA, human kallikrein 2 (hK2; *KLK2*) is a prostate gland- and cancer cell-specific trypsin-like serine protease that is tightly governed by the functional status of the androgen receptor (AR) hormone response circuit, and is elevated in the serum of >20% of patients following EBRT⁹. We previously developed 11B6, an IgG1 antibody with high selectivity and specificity for the active cleavage site of hK2. 11B6 uniquely binds to hK2 directly at the cell surface – i.e., at the site of hK2 production and thus, AR activity - and avoids interaction with serum kallikreins. When derivatized with medically relevant radionuclides, this platform can be used for radio-immunotheranostics for detection, delineation, and treatment of diverse models of AR-expressing adenocarcinoma^{10–12}. Positron emission tomography (PET) with [⁸⁹Zr]11B6 enables monitoring of prostate cancer growth (PCa) and quantification of lesion-specific AR-activity^{10–12}.

We hypothesize that [⁸⁹Zr]11B6-PET can be used to noninvasively monitor EBRT-induced changes in AR-activity in individual PCa lesions. Using quantitative imaging and genomic analyses of human xenograft and genetically engineered mouse models of PCa, EBRT-induced AR activity was visualized and correlated to transcriptomic alterations following therapy with near-term implications for PCa treatment paradigms.

Materials and Methods

Radiochemistry

Radiosynthesis of [⁸⁹Zr]-DFO-11B6 ([⁸⁹Zr]11B6) has previously been described¹³. 11B6 antibody was provided by Dr. Kim Pettersson, University of Turku, Finland. All labeling reactions achieved >99% radiochemical purity. Average specific activity of the final radiolabeled conjugate was 51.8 MBq/mg (1.4 mCi/mg).

Cell lines

22Rv1 cells were purchased from ATCC. LNCaP-AR (LNCaP with overexpression of wildtype AR) was a kind gift from Charles Sawyers¹⁴. Cells were cultured according to the providers' instructions and frequently tested for mycoplasma contamination. Cell lines were authenticated using GenePrint10 Short Tandem Repeat analysis (Laragen Inc, Culver City, CA)

Mouse models

All animal experiments were conducted in compliance with MSKCC guidelines, IACUC-established guidelines, and RARC animal protocol (# 04–01-002). Xenografts were established in male athymic BALB/c (nu/nu) mice (6–8 weeks old, 20–25 g; Charles River) by subcutaneous injection of LNCaP-AR or 22Rv1 cells (1–5×10⁶ cells, 1:1 = media : Matrigel). Tumors developed after 3–7 weeks. The transgenic PCa mouse models used, Hi-*Myc* × Pb-*KLK2* with prostate-specific AR-driven hK2 expression, as well as Pb-*KLK2* mice with abundant AR-driven hK2 expression specific to murine prostate tissue, have been previously reported¹⁰. Irradiated animals ranged from 35–42 weeks at study outset.

EBRT

Irradiation of disease sites was performed as previously described¹⁵. Briefly, a whole-body CT was acquired (XRad225Cx, Precision X-Ray, Inc.; dual focal spot x-ray tube at 45 kVp with a flat-panel amorphous silicon imager mounted on a C-arm gantry), tumor fields were identified and a treatment plan with >3 angles and a dose rate of \$3 Gy/min (tube voltage, 225 kVp) was devised. Radiation dosimetry was performed using Gafchromic EBT film (ISP Inc.); a clear film that polymerizes with increasing optical density to a degree linearly with dose. The Gafchromic film verified the targeting accuracy, the magnitude of dose delivered and the geometry of the planned dose plan.

Magnetic resonance imaging

Prostate tumor volumes were defined using T2-weighted MR scans (Bruker BioSpin 4.7 T). An interleaved T2-weighted turbo spin echo sequence (3,200/57.1) with 8 averages was used, with slice dimensions of $8.5 \times 3.99 \times 0.8$ cm. A total scan duration of 10 minutes 14 seconds generated 220 μ m and 800 μ m in and out of plane slices, respectively. A trained reader calculated prostate volumes by segmenting the prostate (OsiriX, v8.1)¹⁶.

Gene expression analysis

RNA was purified using the RNeasy Mini Kit (Qiagen), and quantitative PCR to determine expression of *KLK2*, *KLK3*, and *FOLH1* was performed as previously described.

For RNA-sequencing, raw read count RNA-sequencing data were generated from untreated (NT; n = 3) LNCaP-AR tumor samples and 5×10 Gy (n=3) treated samples. A total of 58,828 genes were acquired and analyzed as previously reported¹⁷. Both hierarchical clustering analysis (based on Euclidean distance) and multi-dimensional scaling (MDS) plots demonstrated a clear division between the samples from the two cohorts (Suppl. Fig. 1, 2). Differentially expressed genes (DEGs) were defined at an adjusted $p < 0.001$ and an absolute value of \log_2 fold-change > 1 . A positive fold-change represented up- and a negative fold change represented downregulation in EBRT-treated tumors. Pathway analysis was performed using enrichR¹⁸ and the KEGG 2021 database.

Bioluminescence imaging

Activity of the AR-dependent reporter construct expressed in LNCaP-AR tumors was quantified by bioluminescence imaging (Living Image[®] 4.5.2) following retro-orbital injection of D-Luciferin (30 mg/mL, 10 μ L; exposure times 1, 5, 10, 20, and 40 seconds). Data were expressed as radiance (photons/s) divided by tumor volume measured by caliper ($V = \text{length} \times \text{width}^2$).

Impact of EBRT on [⁸⁹Zr]11B6 tumor uptake

Mice bearing LNCaP-AR and 22Rv1 xenografts, and Hi-*Myc* \times Pb-*KLK2* and Pb-*KLK3* mice, received [⁸⁹Zr]11B6 (3.7–5.55 MBq [100–150 μ Ci], 25 μ g protein, i.v.; t=0 h), after EBRT (n=4–5/group). To confirm specificity, a control group of mice with 22Rv1 tumors treated with 4×5 Gy was co-injected with 1 mg of unlabeled 11B6. [⁸⁹Zr] radioactivity in tumors and organs harvested 120 h post-injection (p.i.) was quantified using a gamma-

counter. Data were background and decay corrected, and the percentage injected activity per gram tissue (%IA/g) was calculated.

Monitoring AR-activity using PET/ CT

PET/CT imaging (Inveon MM, IRW Acquisition software) was performed as previously described¹⁹, at 120 h p.i. with Hi-*Myc* × Pb-*KLK2* following administration of [⁸⁹Zr]11B6 (3.7–5.55 MBq [100–150 µCi], 25 µg of protein, i.v.). Duration of PET scans were 1 h or until 20×10^6 coincident events were recorded. A 3D maximum a priori reconstruction was used to generate tomographic datasets. Assessment of hK2 expression for correlation with [⁸⁹Zr]11B6 uptake was reported previously¹⁷.

Histology

Prostate tissues of Hi-*Myc* × Pb-*KLK2* and Pb-*KLK2* mice harvested after EBRT (5 × 10 Gy) were fixed in 4% paraformaldehyde and cut into 15 µm sections before staining with hematoxylin and eosin (H&E). Immunohistochemistry (IHC) for detection of AR and c-MYC was performed at the Molecular Cytology Core Facility (MSKCC) using a Discovery XT processor (Ventana Medical Systems). Sections were blocked in 10% normal goat serum in PBS for 30 minutes before staining with an anti-AR (N-20) antibody (1 µg/mL, 3 h; Santa Cruz, #SC-816; secondary: biotinylated goat anti-rabbit IgG, 1:200, 16 minutes; Vector labs, #PK6101), or an anti-c-MYC antibody (1:100, 5h; Epitomics, #P01106; secondary: biotinylated goat anti-rabbit IgG, 1:200, 1 h; Vector labs, #PK6101). Blocker D, Streptavidin-HRP and DAB detection kit (Ventana Medical Systems) were used according to the manufacturer's instructions.

Statistics

Statistical significance was determined by unpaired two-tailed t-test (2 groups) or, for >2 groups, by one-way ANOVA followed by Dunnett's test to correct for multiple comparisons and set to $p < 0.05$. Data are presented as mean ± standard deviation (SD). Analysis was performed with GraphPad Prism Version 9.2.0. For RNA-sequencing, differentially expressed genes were considered significant with an adjusted $p < 0.001$ and log₂ fold-change >1 as described previously¹⁷.

Data availability statement

The RNA-sequencing data reported in this paper have been deposited in the Gene Expression Omnibus (GEO) database, <https://www.ncbi.nlm.nih.gov/geo> (accession no.GSE206847). Other data generated in this study are available upon request from the corresponding author.

Results

Changes in AR and AR-driven PCa biomarkers in response to EBRT

PCR analysis of LNCaP-AR tumors treated with 1, 3 or 5 fractions of 2, 5 or 10 Gy EBRT revealed dose-dependent increases in *AR*, *KLK2*, *KLK3* compared to nontreated (NT) controls (**Fig. 1, Table 1**). *FOLH1* expression after EBRT varied and remained

unchanged under EBRT (**Fig. 1B, Table 1**). After 3 cycles of EBRT in 22Rv1 xenografts, *AR* gene expression was significantly increased along with *KLK2* and *KLK3*, while there were no significant changes in *FOLH1* expression (**Fig. 1C, Table 1**). The fold change of *AR* transcription was higher in 22Rv1 than LNCaP-AR tumors, which is likely an effect of lower baseline *AR* expression in the 22Rv1 model. This outcome corresponds with previously reported findings and provides additional support for the correlation between *KLK2* and *AR* expression when monitoring changes rendered by EBRT⁹.

Investigating EBRT-induced transcriptomic changes in an unbiased approach, 4,851 DEGs (8.2% of transcriptome gene set) were identified in LNCaP-AR tumors after EBRT (5 × 10 Gy; vs. NT); 2,552 genes were up- and 2,299 were downregulated (Fig. 2). Upregulation of *AR*-regulated genes such as *AR* signaling co-activator *ETV1*²⁰, *KLK2*, and *KLK3* (log₂ fold-change= 10.01, 1.033, 1.882) indicated that *AR* signaling was increased after EBRT. Interestingly, other *AR* target genes, including *TMPRSS2* and *FKBP5*, were downregulated following treatment. Of the 144 previously established *AR*-associated DNA repair genes²¹, 18 were DEGs with 8/18 upregulated (*CHEK1*, *FANCL*, *MAD2L1*, *MBM7*, *PARP1*, *RAD18*, *RAD21*, *RFC3*)^{21,22}. *FOLH1* was also upregulated despite its inverse correlation to *AR* pathway activity, contrasting qPCR findings. Upregulated *MYC* expression in EBRT-treated tumors supports a role for *MYC* in *AR*-driven EBRT responses, and pathway analysis showed that the top DEGs converged on cell cycle and regulation of DNA replication, both of which are closely intertwined with *AR* through cyclins and changes in protein expression during replication^{23,24}, further supporting a role for *AR* signaling in PCa response to EBRT.

EBRT increases AR activity in PCa *in vivo*

To confirm EBRT-induced *AR* signaling *in vivo*, activation of an *AR*-reporter gene in LNCaP-AR tumors was assessed using bioluminescence imaging. EBRT increased mean *AR*-activity without significant differences between 1 and 4 fractions (Fig. 1D).

[⁸⁹Zr]11B6-uptake is an indicator of EBRT-induced AR activity

[⁸⁹Zr]11B6 tissue uptake was assessed in 22Rv1 and LNCaP-AR tumors treated with 2, 5 or 10 Gy (1 or 4 fractions) EBRT or left untreated (Fig. 3). A total EBRT dose >10 Gy significantly increased uptake of [⁸⁹Zr]11B6 by LNCaP-AR tumors (38.61–47.24 %IA/g vs. 17.9%–28.3 %IA/g in NT) and 22Rv1 xenografts (13.2–62.6 %IA/g, vs. 7.9–11.2 %IA/g NT). Co-injection of cold 11B6 significantly decreased [⁸⁹Zr]11B6-uptake by 22Rv1 tumors after 20Gy EBRT (13.2–21.9 %IA/g vs 2.1–13.2 %IA/g blocked), confirming hK2 specificity (Fig. 3B).

EBRT-induced AR activity in PCa can be monitored by [⁸⁹Zr]11B6 positron emission tomography (PET) / computed tomography (CT) imaging

To confirm [⁸⁹Zr]11B6 uptake as a surrogate marker for EBRT-induced *AR* activity, [⁸⁹Zr]11B6 uptake was quantified *in vivo* and *ex vivo* in Pb-*KLK2* (non-malignant) and Hi-*Myc* x Pb-*KLK2* (PCa) mice after treatment with 5 fractions of 10 Gy. No significant volumetric changes were observed by MRI (**Fig. 4A,B**) after EBRT treatment of PCa tissue. EBRT increased *AR* expression in PCa (Hi-*Myc* x Pb-*KLK2*) (Fig. 4C); this was paralleled

by significantly higher [⁸⁹Zr]11B6 uptake after EBRT *in vivo* (before EBRT, 11.04 ± 4.42%; after EBRT (same cohort of mice), 20.23 ± 4.28%).

In contrast, EBRT did not impact uptake in Pb_*KLK2* mice (Fig. 5A-C). Correlation of hK2 protein levels in tumors and [⁸⁹Zr]11B6-uptake further confirmed AR activity (Fig. 5D). Taken together, these results indicate that hK2-targeted [⁸⁹Zr]11B6 can noninvasively monitor increased AR signaling after radiotherapy in a *Myc*-driven model of PCa.

Discussion

The current study demonstrates that EBRT-induced AR-activity, which increases in a dose-dependent manner, can be monitored noninvasively using PET. Activation of AR-signaling by EBRT may serve as prognostic biomarker and improve development of EBRT combination regimens. In a phase 3 clinical trial, the combination of EBRT with bicalutamide increased disease-free survival²⁵, and PSA decay rate during salvage radiotherapy has been identified as a predictor of progression-free survival²⁶. EBRT-induced AR-activity might thus negatively impact patient outcomes, and vice versa, inhibition of this response may improve patient care. Attempts to monitor AR noninvasively have been made with [¹⁸F]FDHT, a radio-analog of testosterone²⁷; however, [¹⁸F]FDHT reports AR levels rather than its functional signaling activity. To measure AR pathway activity, several AR target genes are utilized as biomarkers and therapeutic targets in PCa, including prostate-specific membrane antigen (PSMA) and PSA. Recently, FDA-approved PSMA-PET has increased the ability to detect metastatic PCa lesions and is considered as a strategy to monitor AR blockade by ADT. Unfortunately, preclinical and clinical studies demonstrated that PSMA-PET is not an optimal tool for assessment of ADT efficacy²⁸⁻³¹. We observed similar findings in our evaluation of PSMA levels after EBRT; *FOLH1* expression increased 2.5-fold in 22Rv1 but not in LNCaP-AR xenografts. Taken together, these results underline the complex links between AR-activity, EBRT resistance, and AR pathway biomarkers. It should however be noted that resistance to EBRT may also be caused by non-AR driven mechanisms.

KLK2 expression and corresponding hK2 protein levels are well-established as biomarkers of AR pathway activity^{9,10}. In line with a previous study⁹, we showed that EBRT increases *KLK2* expression in a dose-dependent manner. To noninvasively target *KLK2* expressing cells, we developed 11B6, an antibody that specifically internalizes into PCa cells in response to AR-activity by binding uncomplexed hK2¹⁰. 11B6 can be exploited for PET, single photon emission tomography, intra-operative imaging^{10,13}, and radioimmunotherapy^{18,26,40-41}. Studies in multiple rodent models and non-human primates showed that [⁸⁹Zr]11B6 rapidly accumulates in PCa¹¹, and changes in PCa [⁸⁹Zr]11B6-uptake correspond to both AR-activity and hK2 protein levels¹⁰. We thus hypothesized that [⁸⁹Zr]11B6 could be used to monitor changes in AR-activity during and after EBRT. We confirmed relevance of [⁸⁹Zr]11B6-uptake as biomarker by correlating its tumor-uptake with EBRT-induced expression of the canonical AR biomarker *KLK2*. Furthermore, EBRT did not increase [⁸⁹Zr]11B6 prostate uptake in healthy Pb_*KLK2* mice while uptake was significantly elevated in PCa of Hi-*Myc* x Pb_*KLK2* mice; this suggests that EBRT-induced AR activation is a radiobiological response unique to malignant prostate tissues.

EBRT-induced AR activation exclusively in PCa-bearing mice as well as elevated *MYC* levels in xenografts and c-MYC expression in the genetic PCa model after EBRT support the known relationship between MYC and AR. MYC upregulation has been shown to antagonize AR signaling and AR target gene expression in patient samples³² but has been positively correlated to AR variant expression in another study³³. Upregulation of MYC may provide rationale for the use of co-treatment concepts using direct or indirect MYC inhibitors to block additional pro-tumorigenic transcription factors that drive PCa³⁴.

The difference in [⁸⁹Zr]11B6 uptake in the LNCaP-AR xenograft tumor model and the well-documented role of AR as a transcription factor led us to hypothesize that there would be a significant transcriptomic impact in the post EBRT-treatment setting. However, analysis of RNA-sequencing of irradiated mice revealed a downregulation of AR, highlighting the variability in tissue response to EBRT. This result exemplifies the need for diagnostic agents that focus on assessing functional AR pathway activity rather than the number of available receptors or AR expression itself. Upregulation of AR pathway target genes *KLK2* and *KLK3* in our data clearly demonstrate that the AR pathway is being differentially activated in tumor-bearing mice after radiotherapy.

The transcriptional EBRT-signature observed in the current study is in line with that reported for 11B6 alpha-radioimmunotherapy in Hi-*Myc* x Pb-*KLK2* mice¹⁷. Comparison of the top ten up- and downregulated DEGs revealed five common up- (*MMP7*, *ETV1*, *NTS*, *PLA2G2A*, *PEG3*) and down-regulated DEGs (*PASD1*, *DENN2D*, *PTGFR*, *SLC25A43*, *FAM213A*); this similarity underscores the ability of [⁸⁹Zr]11B6-PET to reflect AR-driven therapeutic responses.

Overall, we demonstrated a highly specific and sensitive approach for noninvasive monitoring of functional AR-activity under EBRT. We propose that a baseline hK2-PET would be utilized at the time of dose planning, with repeated imaging following treatment start to monitor AR-signal. Exclusively in cancerous tissue, [⁸⁹Zr]11B6 tumor-uptake correlated with AR pathway activation after irradiation. Changes in [⁸⁹Zr]11B6 PCa-uptake paralleled increases in *KLK2* and *AR* expression seen in qPCR analysis, as well as *ex vivo* hK2 protein concentrations and IHC staining. The significantly shorter circulation time of the 11B6 mAb construct in humans (and non-human primates) compared to mice supports feasibility of serial imaging³⁵ in patients.

Most patients receive co-treatment with pharmacological compounds inhibiting the AR-pathway. However, in some lesions the AR-pathway is still active to some degree due to insufficient dosing, and unknown resistance mechanisms and pathobiology. In this scenario, the molecularly specific and spatially defined signal of 11B6-PET may indicate areas that should receive increased radiation, or conversely, areas without (remaining) hK2-PET signal could be de-escalated to reduce risk of radiation-induced toxicity to surrounding tissues. The notion that rodents have about 50-fold lower testosterone levels than humans, rather than par with castrated patients, underlines the utility of this molecular, lesion-specific, cancer imaging strategy.

There is no doubt that the cost of imaging is a contentious issue in modern patient management. However, the cost of a PET scan (or multiple scans) relative to the treatment planning scans and daily radiation dosing is incremental – and the ability to capture personalized precision information of patient response (in particular AR-active lesions that may be outside of the prescribed dose field) is capable of driving significant long term cost savings. Therefore, hK2-PET/CT would facilitate a deeper understanding of response and resistance patterns of individual tumor lesions and patients and ultimately, of how to adjust treatment.

Thus, although clinical trials are needed, monitoring the AR-target gene hK2 in the treatment setting could allow patient stratification based on AR-pathway response, refinement of treatment and dosing strategies, e.g., by selection of AR-targeted treatment combinations and allowing physicians to prescribe the lowest dose needed, and may provide mechanistic insights into enhancement of EBRT in some patients with concurrent or adjuvant ARSI.

Supplementary Material

Refer to Web version on PubMed Central for supplementary material.

Acknowledgements

We thank Drs. Brent Rupnow, Marco Gottardis, and Michael Russell at oncology innovation at the Janssen pharmaceutical companies of Johnson & Johnson for excellent discussions and intellectual input, and Janssen R&D LLC for partially funding the studies.

Financial support:

This study was supported in part by the UCLA Eli and Edythe Broad Center of Regenerative Medicine and Stem Cell Research Rose Hill Foundation Innovator Award, the Imaging and Radiation Sciences Program, U.S. NIH grant P30 CA008748 (MSKCC Support Grant). The MSKCC Small-Animal Imaging Core Facility is supported in part by NIH grants P30 CA008748–48, S10 RR020892–01, S10 RR028889–01, and the Geoffrey Beene Cancer Research Center. We also acknowledge William H. Goodwin and Alice Goodwin and the Commonwealth Foundation for Cancer Research, the Experimental Therapeutics Center, and the Radiochemistry & Molecular Imaging Probe Core (P50-CA086438), all of MSKCC. M.R. McDevitt: NIH R01CA166078, R01CA55349, P30CA008748, P01CA33049, F31CA167863, the MSKCC for Molecular Imaging and Nanotechnology. S. Larson: Ludwig Center for Cancer Immunotherapy (MSKCC), NCI P50-CA86438. H. Lilja: NIH/NCI CCSG to MSKCC (P30 CA008748), NIH/NCI P50CA092629 and R01 CA244948 Sidney Kimmel Center for Prostate and Urologic Cancers. David H. Koch Prostate Cancer Foundation Award, Swedish Cancer Society (Cancerfonden 20 1354 PjF), Swedish Research Council (VR-MH 2016–02974), General Hospital in Malmö Foundation for Combating Cancer. D.L.J. Thorek: NCI R01CA201035, R01CA240711, R01CA229893. D. Ulmert, M.R. McDevitt: DoD W81XWH-18–1-0223. D. Ulmert: UCLA SPORE in Prostate Cancer (P50 CA092131), JCCC Cancer support grant from NIH P30 CA016042 (PI: Teitell), Knut and Alice Wallenberg Foundation, Bertha Kamprad Foundation, David H. Koch Prostate Cancer Foundation Young Investigator Award, Swedish Cancer Society, and Swedish Cancer Foundation.

C. Storey is named on a patent in the field of radioimmunotherapy and drug delivery pending, licensed, and with royalties from Radiopharm Theranostics. M. Altai reports grants from Swedish Cancer Foundation, Kamprad Foundation and Lund University, Lundberg Foundation and Bergqvist Foundation; is a consultant for Genagon AB and Pharma15 C-Corp. K. Lückerath reports personal fees from Sofie Biosciences outside the submitted work. R. Damoiseaux reports a patent for Antibodies pending. S.M. Larson reports grants from NIH during the conduct of the study, and grants from YMABS Therapeutics Inc and royalties from Elucida, SAMOS, and YMABS Therapeutic Inc outside the submitted work; in addition, S.M. Larson has several patents in the field of Radioimmunotherapy and Drug delivery pending, issued, licensed, and with royalties paid from YMABS Therapeutic; a patent for Nanoparticles issued, licensed, and with royalties paid from Elucida Inc; and a patent for radiotracer drugs from SAMOS; and reports consultation regarding drug products with Progenics, Janssen, and Exini (Lantheus) during the conduct of this work and preparation of article. H. Lilja is named on patents for intact

PSA assays and a statistical method to detect prostate cancer (4KScore test) that has been commercialized by OPKO Health; receives royalties and has stock in OPKO Health; has been a consultant to Diaprost AB and has stock in Diaprost AB; and has received a speakers' honorarium from Janssen R&D LLC. D.L.J. Thorek reports grants from NIH NCI (R0128335, R0128238, R0128539) during the conduct of the study and is scientific advisor for and has equity in Diaprost AB and Pharma15. D. Ulmert reports grants from Prostate Cancer Foundation, Rosehill Foundation, Eli and Edythe Broad Center of Regenerative Medicine and Stem Cell Research, Kamprad Foundation, Swedish Research Foundation, Swedish Cancer Foundation, Sanofi Innovation, Janssen R&D LLC, and Department of Defense during the conduct of the study; has several patents in the field of Radioimmunotherapy and Drug delivery pending, issued, licensed, and with royalties paid from YMABS Therapeutic, Radiopharm Theranostics, and Diaprost AB outside the submitted work; is a consultant for Astra Zeneca, Two River, Ferring Ventures, Vida Ventures, Novartis Ventures, Genagon AB, Pharma15 C-Corp, and Diaprost AB.

References

1. Arora VK et al. Glucocorticoid receptor confers resistance to antiandrogens by bypassing androgen receptor blockade. *Cell* 155, 1309–1322 (2013). [PubMed: 24315100]
2. Handle F. et al. Drivers of AR indifferent anti-androgen resistance in prostate cancer cells. *Sci. Rep.* 9, 13786 (2019). [PubMed: 31551480]
3. Antonarakis ES et al. AR-V7 and resistance to enzalutamide and abiraterone in prostate cancer. *N. Engl. J. Med.* 371, 1028–1038 (2014). [PubMed: 25184630]
4. Zhu Y. et al. Role of androgen receptor splice variant-7 (AR-V7) in prostate cancer resistance to 2nd-generation androgen receptor signaling inhibitors. *Oncogene* 39, 6935–6949 (2020). [PubMed: 32989253]
5. Bolla M. et al. External irradiation with or without long-term androgen suppression for prostate cancer with high metastatic risk: 10-year results of an EORTC randomised study. *Lancet Oncol.* 11, 1066–1073 (2010). [PubMed: 20933466]
6. Widmark A. et al. Endocrine treatment, with or without radiotherapy, in locally advanced prostate cancer (SPCG-7/SFUO-3): an open randomised phase III trial. *Lancet* 373, 301–308 (2009). [PubMed: 19091394]
7. Ulmert D., O'Brien MF, Bjartell AS & Lilja H. Prostate kallikrein markers in diagnosis, risk stratification and prognosis. *Nat. Rev. Urol.* 6, 384–391 (2009). [PubMed: 19578355]
8. Sävbom C. et al. Blood levels of free-PSA but not complex-PSA significantly correlates to prostate release of PSA in semen in young men, while blood levels of complex-PSA, but not free-PSA increase with age. *Prostate* 65, 66–72 (2005). [PubMed: 15880475]
9. Spratt DE et al. Androgen Receptor Upregulation Mediates Radioresistance after Ionizing Radiation. *Cancer Res.* 75, 4688–4696 (2015). [PubMed: 26432404]
10. Thorek DLJ et al. Internalization of secreted antigen-targeted antibodies by the neonatal Fc receptor for precision imaging of the androgen receptor axis. *Sci. Transl. Med.* 8, 367ra167 (2016).
11. McDevitt MR et al. Feed-forward alpha particle radiotherapy ablates androgen receptor-addicted prostate cancer. *Nat. Commun.* 9, 1629 (2018). [PubMed: 29691406]
12. Thorek DLJ et al. Harnessing Androgen Receptor Pathway Activation for Targeted Alpha Particle Radioimmunotherapy of Breast Cancer. *Clin. Cancer Res.* 25, 881–891 (2019). [PubMed: 30254080]
13. Timmermand OV et al. Preclinical imaging of kallikrein-related peptidase 2 (hK2) in prostate cancer with a (111)In-radiolabelled monoclonal antibody, 11B6. *EJNMMI Res.* 4, 51 (2014). [PubMed: 26116115]
14. Chen CD et al. Molecular determinants of resistance to antiandrogen therapy. *Nat. Med.* 10, 33–39 (2004). [PubMed: 14702632]
15. Thorek DLJ et al. Reverse-Contrast Imaging and Targeted Radiation Therapy of Advanced Pancreatic Cancer Models. *Int. J. Radiat. Oncol. Biol. Phys.* 93, 444–453 (2015). [PubMed: 26238952]
16. Rosset A., Spadola L. & Ratib O. OsiriX: an open-source software for navigating in multidimensional DICOM images. *J. Digit. Imaging* 17, 205–216 (2004). [PubMed: 15534753]
17. Bica M. et al. Genetic signature of prostate cancer mouse models resistant to optimized hK2 targeted α -particle therapy. *Proc. Natl. Acad. Sci. U. S. A.* 117, 15172–15181 (2020). [PubMed: 32532924]

18. Kuleshov MV et al. Enrichr: a comprehensive gene set enrichment analysis web server 2016 update. *Nucleic Acids Res.* 44, W90–7 (2016). [PubMed: 27141961]
19. Veach DR et al. PSA-Targeted Alpha-, Beta-, and Positron-Emitting Immunotheranostics in Murine Prostate Cancer Models and Nonhuman Primates. *Clin. Cancer Res.* (2021).
20. Baena E. et al. ETV1 directs androgen metabolism and confers aggressive prostate cancer in targeted mice and patients. *Genes Dev.* 27, 683–698 (2013). [PubMed: 23512661]
21. Polkinghorn WR et al. Androgen receptor signaling regulates DNA repair in prostate cancers. *Cancer Discov.* 3, 1245–1253 (2013). [PubMed: 24027196]
22. Sharma NL et al. The androgen receptor induces a distinct transcriptional program in castration-resistant prostate cancer in man. *Cancer Cell* 23, 35–47 (2013). [PubMed: 23260764]
23. Litvinov IV et al. Androgen receptor as a licensing factor for DNA replication in androgen-sensitive prostate cancer cells. *Proc. Natl. Acad. Sci. U. S. A.* 103, 15085–15090 (2006). [PubMed: 17015840]
24. Schiewer MJ et al. Dual roles of PARP-1 promote cancer growth and progression. *Cancer Discov.* 2, 1134–1149 (2012). [PubMed: 22993403]
25. Radiation Therapy With or Without Bicalutamide and Goserelin in Treating Patients With Prostate Cancer. [ClinicalTrials.gov](https://clinicaltrials.gov/ct2/show/study/NCT00021450) identifier: [NCT00021450](https://clinicaltrials.gov/ct2/show/study/NCT00021450) (2016).
26. Gunnlaugsson A. et al. PSA decay during salvage radiotherapy for prostate cancer as a predictor of disease outcome - 5 year follow-up of a prospective observational study. *Clin Transl Radiat Oncol* 24, 23–28 (2020). [PubMed: 32613088]
27. Beattie BJ et al. Pharmacokinetic assessment of the uptake of 16beta-18F-fluoro-5alpha-dihydrotestosterone (FDHT) in prostate tumors as measured by PET. *J. Nucl. Med.* 51, 183–192 (2010). [PubMed: 20080885]
28. Enzalutamide With Lu PSMA-617 Versus Enzalutamide Alone in Men With Metastatic Castration-resistant Prostate Cancer (ENZA-p). [ClinicalTrials.gov](https://clinicaltrials.gov/ct2/show/study/NCT04419402) Identifier: [NCT04419402](https://clinicaltrials.gov/ct2/show/study/NCT04419402) (2022).
29. Lückerrath K. et al. Preclinical evaluation of PSMA expression in response to androgen receptor blockade for theranostics in prostate cancer. *EJNMMI Res.* 8, 96 (2018). [PubMed: 30374743]
30. Staniszewska M. et al. Enzalutamide Enhances PSMA Expression of PSMA-Low Prostate Cancer. *Int. J. Mol. Sci.* 22, 7431 (2021). [PubMed: 34299051]
31. Kuten J., Sarid D., Yossepowitch O., Mabweesh NJ & Even-Sapir E. [68Ga]Ga-PSMA-11 PET/CT for monitoring response to treatment in metastatic prostate cancer: is there any added value over standard follow-up? *EJNMMI Res.* 9, 84 (2019). [PubMed: 31468235]
32. Barfeld SJ et al. c-Myc Antagonises the Transcriptional Activity of the Androgen Receptor in Prostate Cancer Affecting Key Gene Networks. *EBioMedicine* 18, 83–93 (2017). [PubMed: 28412251]
33. Bai S. et al. A positive role of c-Myc in regulating androgen receptor and its splice variants in prostate cancer. *Oncogene* 38, 4977–4989 (2019). [PubMed: 30820039]
34. Llombart V. & Mansour MR Therapeutic targeting of “undruggable” MYC. *EBioMedicine* 75, 103756 (2022).
35. Ober RJ, Radu CG, Ghetie V. & Ward ES Differences in promiscuity for antibody-FcRn interactions across species: implications for therapeutic antibodies. *Int. Immunol.* 13, 1551–1559 (2001). [PubMed: 11717196]

Implications

hK2 expression in PCa tissue is a proxy of EBRT-induced AR activity that can noninvasively be detected using [⁸⁹Zr]11B6-PET; further clinical evaluation of hK2-PET for monitoring response and development of resistance to EBRT in real time is warranted.

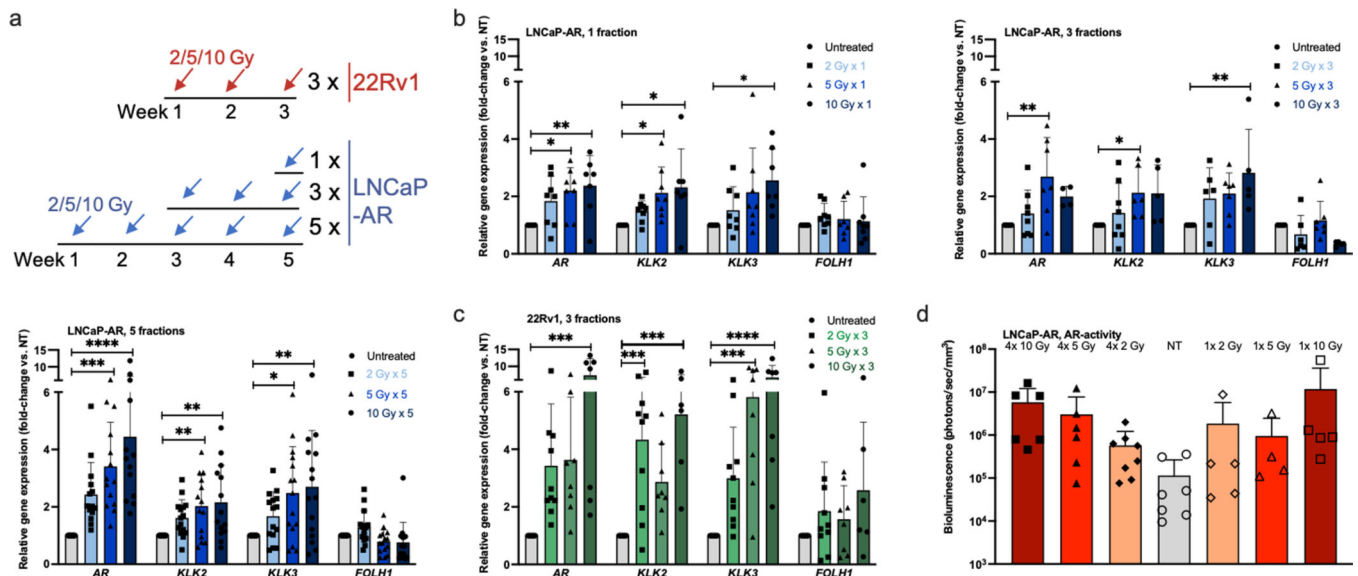


Figure 1. AR activity and gene expression after EBRT in LNCaP-AR and 22Rv1 xenografts. **A**, Schematic of EBRT fractionation regimen. **B,C**, Gene expression analysis of LNCaP-AR (**B**) and 22Rv1 (**C**) xenografts after 1, 3, and 5 fractions of 2, 5 or 10 Gy EBRT revealed upregulation of *AR* and *KLK2/KLK3* in a dose-dependent manner. Data were normalized to NT. See Table 1 for mean and p-values. **D**, Bioluminescence imaging readout of AR activity in LNCaP-AR xenografts after 1 or 4 fractions of EBRT revealed dose-dependent increase in AR activity independent of fractionation (all p=not significant vs. NT). Mean \pm SD and individual values are given; statistical significance was calculated using one-way ANOVA and Dunnett's test for multiple comparisons.

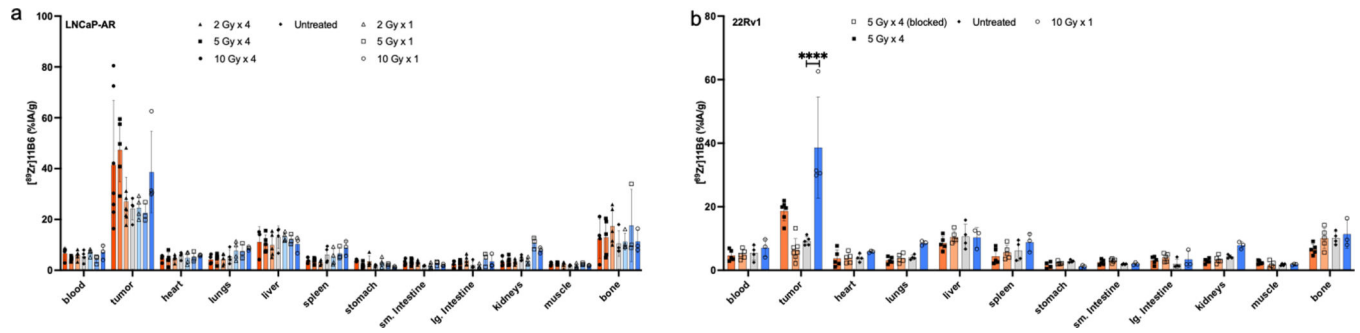


Figure 3. [⁸⁹Zr]11B6 localizes to PCa after irradiation.

Ex vivo biodistribution of [⁸⁹Zr]11B6 in LNCaP-AR (A) and 22Rv1 (B) at 120h post-EBRT revealed higher uptake in irradiated tumors that received more than 8 Gy total dose of EBRT. Cold, unlabeled 11B6 confirmed specificity in 22Rv1. Mean ± SD and individual values are given; statistical significance was calculated for tumor uptake (NT vs. EBRT) using one-way ANOVA and Dunnett's test for multiple comparisons.

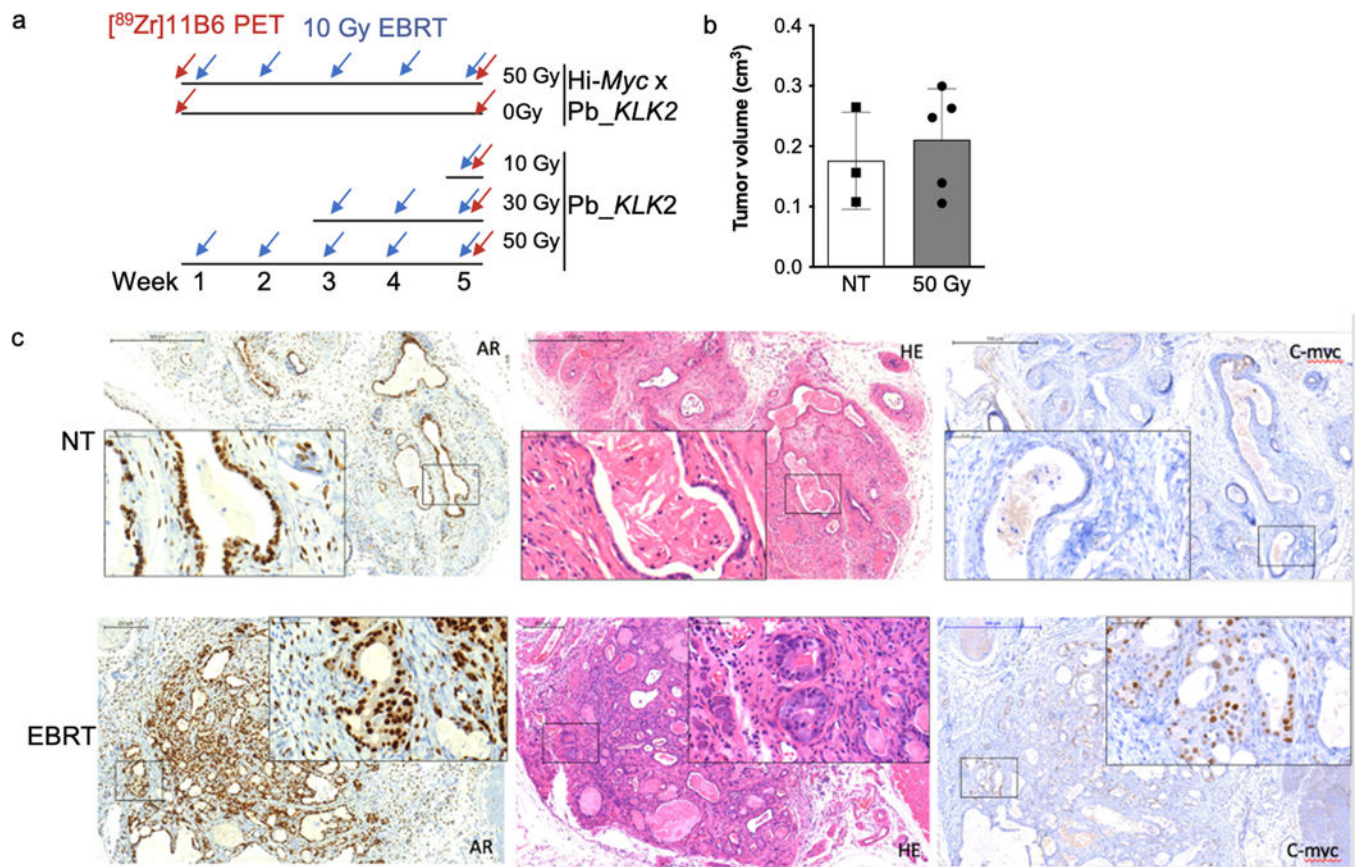


Figure 4. EBRT treatment of Hi-Myc x Pb_KLK2 and Pb_KLK2 mice.

A, EBRT and imaging schedule for PCa (Hi-Myc x Pb_KLK2) and healthy (Pb_KLK2) mice. **B**, MR imaging revealed comparable PCa volumes \pm 50 Gy treatment. Mean \pm SD and individual values are given; statistical significance was calculated using unpaired two-tailed t-test ($p=0.5872$). **C**, IHC of Hi-Myc x Pb_KLK2 tumors revealed increased intratumor AR and c-MYC expression after EBRT (magnification: overview 10x, insert 40x).

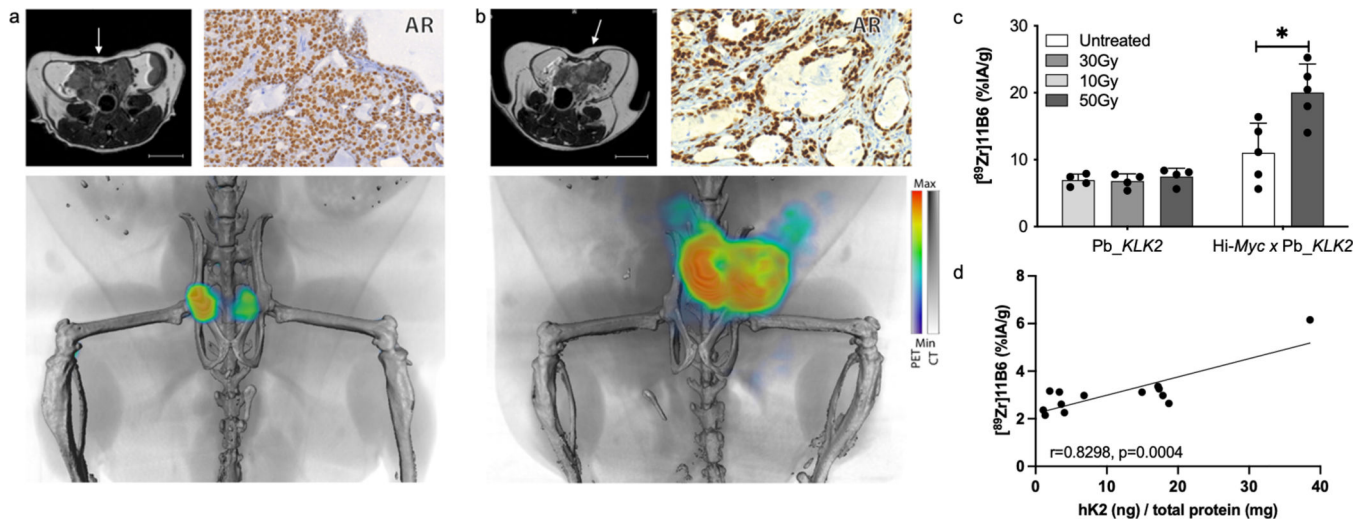


Figure 5. AR activity increase following EBRT visualized by [89Zr]11B6-PET/CT. Representative MR, IHC (40x magnification) and volume rendered PET/CT images before treatment (A) and after irradiation with 50 Gy (B) of a Hi-Myc x Pb_KLK2 mouse. White arrow indicates prostate location in MR images (scale: 0.5 cm). (C) Activity concentration of [89Zr]11B6 increased following irradiation ($p < 0.05$). Mean \pm SD are given; statistical significance was calculated using unpaired two-tailed t-test. (d) PET signal from [89Zr]11B6 corresponds with *ex vivo* hK2 expression.

Table 1.
Fold-change of AR and AR pathway genes in LNCaP-AR and 22Rv1 tumors after EBRT
(vs. controls).

Mean ± SD are given; p-values (treatment vs. NT) are shown in parentheses and were calculated using one-way ANOVA and Dunnett’s test for multiple comparisons.

	1 Fraction	2 Gy	5 Gy	10 Gy
LNCaP-AR	<i>Ar</i>	1.8 ± 0.9 (0.1044)	2.2 ± 0.8 *(0.0128)	2.4 ± 1.0 **(0.0057)
	<i>Klk2</i>	1.5 ± 0.4 (0.4988)	2.1 ± 0.9 *(0.0248)	2.3 ± 1.3 *(0.0102)
	<i>Klk3</i>	1.5 ± 0.8 (0.6229)	2.1 ± 1.5 (0.0855)	2.6 ± 1.1 *(0.0183)
	<i>Folh1</i>	1.3 ± 0.4 (0.5323)	1.2 ± 0.6 (0.8127)	1.1 ± 0.8 (0.9315)
	3 Fractions	2 Gy	5 Gy	10 Gy
	<i>Ar</i>	1.4 ± 0.8 (0.6799)	2.7 ± 1.4 **(0.0022)	2.0 ± 0.4 (0.1640)
	<i>Klk2</i>	1.4 ± 1.0 (0.6169)	2.1 ± 0.9 *(0.0471)	2.1 ± 1.0 (0.0688)
	<i>Klk3</i>	1.9 ± 1.1 (0.1771)	2.1 ± 0.7 (0.0737)	2.8 ± 1.5 **(0.0052)
	<i>Folh1</i>	0.7 ± 0.7 (0.4646)	1.2 ± 0.7 (0.8600)	0.3 ± 0.1 (0.0615)
	5 Fractions	2 Gy	5 Gy	10 Gy
	<i>Ar</i>	2.4 ± 1.1 (0.0637)	3.4 ± 1.5 *** (0.0008)	4.4 ± 2.8 **** (<0.0001)
	<i>Klk2</i>	1.6 ± 0.6 (0.1540)	2.0 ± 1.1 *(0.0079)	2.2 ± 1.3 *(0.0025)
	<i>Klk3</i>	1.7 ± 0.8 (0.3805)	2.5 ± 1.6 *(0.0104)	2.7 ± 2.0 *(0.0028)
<i>Folh1</i>	1.3 ± 0.6 (0.2652)	0.8 ± 0.4 (0.5133)	0.8 ± 0.7 (0.4302)	
22Rv1	3 Fractions	2 Gy	5 Gy	10 Gy
	<i>Ar</i>	3.4 ± 2.2 (0.1296)	3.6 ± 2.2 (0.1180)	7.3 ± 5.0 *** (0.0001)
	<i>Klk2</i>	4.3 ± 2.5 *** (0.0007)	2.9 ± 1.3 (0.0894)	5.2 ± 2.3 *** (0.0002)
	<i>Klk3</i>	3.0 ± 1.8 (0.1732)	5.8 ± 3.2 *** (0.0005)	6.7 ± 3.5 **** (<0.0001)
	<i>Folh1</i>	1.9 ± 1.7 (0.4425)	1.6 ± 1.2 (0.7579)	2.6 ± 2.4 (0.1146)